INHIBITION OF FOULING WITH TITANIA AND SILICA COATINGS ON PLATE HEAT EXCHANGER IN 80°C SIMULATED GEOTHERMAL WATER

F. Zhang[1], M.Y. Liu[1, 2 *] and W.D. Zhou[1]

[1] Collaborative Innovation Center of Chemical Science and Engineering (Tianjin), School of Chemical Engineering and Technology, Tianjin University, Tianjin 300350, China;
*Corresponding author: myliu@tju.edu.cn.
[2] State Key Laboratory of Chemical Engineering (Tianjin University), Tianjin 300350, China.

ABSTRACT

Coating a barrier layer of certain materials on the surface is a method to prevent fouling on the surfaces of heat exchangers in the geothermal energy utilization system. In this study, Titania (TiO_2), Silica (SiO_2), TiO_2-Fluoroalkylsilane (FPS) and SiO_2-FPS material coatings on AISI 304 SS plates were prepared by liquid phase deposition and sol-gel techniques. A setup of plate heat exchanger with data acquisition system was established to evaluate the antifouling characteristics of coated plates in the convection heat transfer of simulated geothermal water. Antifouling results were obtained on TiO_2-FPS coatings by liquid phase deposition. Corrosion occurred on coatings of TiO_2 and TiO_2-FPS by sol-gel method. The increase of fouling induction period and decrease of final fouling thermal resistance for the coatings of SiO_2 and SiO_2-FPS materials by sol-gel method were not obtained. However, loose deposit on these coatings breaks easier and is easily washed away by geothermal water flow.

INTRODUCTION

Compared with the traditional energy sources, geothermal energy is a highly competitive new energy source with properties of widely distributed, low-cost, directly use and little environmental pollution. It is being widely used in the fields of power generation, district heating, chemical and process industries (Fridleifsson, 2001; Eliasson, et al., 2003; Hepbasli and Ozgener, 2004; Hepbasli,2008; Axelsson et al.,2010; Zheng et al.,2010). Due to the movement of the earth crust, geothermal water has a complex chemical composition. Fouling components include Ca^{2+}, Mg^{2+}, HCO_3^-, SO_4^{2+} and SiO_2. When the geothermal water flows through the device, inorganic salts will form and precipitate on the wall surfaces of the pipes and heat exchanger equipment. Fouling layer deposited on the heat transfer plate increases the flow resistance of the geothermal fluid, decreases the efficiency of heat transfer equipment. Energy consumption increases (Milanovic, et al., 2006). Corrosive components including dissolved O_2, SO_4^{2-}, Cl^-, H^+, sulfide (H_2S, HS^-, S^{2-}) lead to serious corrosion and damaging of the pipe and heat transfer system. Therefore, anti-fouling and anti-corrosion study has great practical significance in the utilization of geothermal energy (Pátzay, et al., 2003; Schmitt,2009; Regenspurg et al., 2010; Kaya, et al., 2011).

In the process industry, chemical routes such as adding chemical inhibitor (Zhang, 1992; Gallup, 2002; Gallup and Barcelon, 2005; Siega, et al., 2005) and physical methods such as cleaning mechanically and exerting physical external fields to the systems are commonly applied to eliminate or prevent fouling (Cho, 1998;Amr, 2000). However, these measures have some problems such as high costs and possible environmental pollution. Studies have shown that the formation or adhesion of fouling particles to a metal surface is a result of the interaction between fouling and heat transfer surface. The adhesion trend is related to the surface free energy of surface materials and generally low surface free energy means low fouling deposition rate on the surface. Surface coating is an effectively technology that can reduce the surface free energy. Low fouling deposition performance on TiO_2 coatings with nano-scale thicknesses obtained by liquid-phase deposition (LPD) method on the substrates of AISI304 stainless steel (SS) was reported (Cai and Liu, 2012). But exceptions were also presented (Zettler, et al., 2005). On a plate heat exchanger in calcium sulfate solution, no significant correlation between surface free energy and asymptotic fouling resistance was found (Zettler, et al., 2005). SiF^+ ion-implanted surface with minimum surface free energy is not the most effective surface in reducing the fouling resistance of the heat exchanger (Förster, et al.,1999). Modifying heat exchanger surface with polytetrafluoroethylene (PTFE), ceramics, polymers, etc. can effectively reduce the surface free energy and exhibit excellent anti-corrosion performance, however, these coatings provide a significant additional resistance to heat transfer due to their low heat conductivity (Kukulka and Leising, 2010; Xu, et al., 2010). Further investigations on surface coating technologies and materials are needed. The LPD and sol-gel coating methods have several advantages. They require simpler coating

ISBN: 978-0-9984188-0-3; Published online www.heatexchanger-fouling.com

equipment, lower deposition temperature. They are applicable to the substrates with larger size and more complex shape.

In this work, six types of surface coatings were prepared by LPD or sol-gel methods on the plate substrates of AISI 304 SS and surface properties were characterized first. Then antifouling performances on these coated heat transfer plates in the convection heat transfer of simulated geothermal water were experimentally evaluated. Some encouraging results were obtained.

EXPERIMENTAL

Apparatus and materials

A plate heat exchange set-up was established to evaluate the fouling resistance characteristics of different coatings on heat transfer plate, and the schematic diagram is shown in Fig.1. The apparatus mainly comprises a hot fluid circulation system, a cold fluid circulation system and a data acquisition system. The red line indicates the circulation route of the hot stream of simulated geothermal water and the green line represents the circulating route of cooling water.

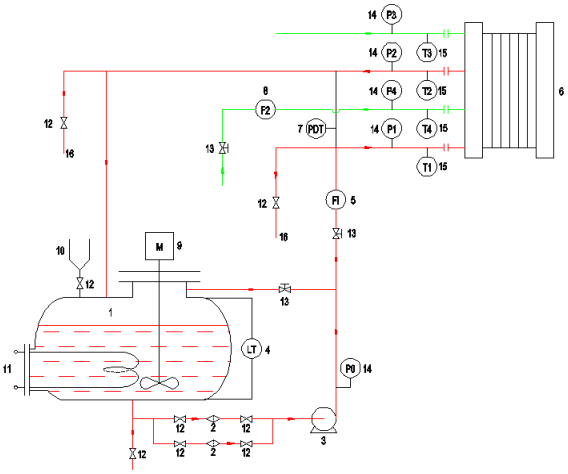

Fig.1 The schematic diagram of plate heat exchange set-up. (1) Geothermal water tank; (2) Y-type filter; (3) Magnetic force pump; (4) Level indicator; (5) Rotameter; (6) Plate heat exchanger; (7) Pressure differential sensor; (8) Electromagnetic flowmeter; (9) Stirrer; (10) Geothermal water inlet; (11) Heating rod; (12) Ball valve; (13) Shut-off valve; (14) Pressure gauge; (15) Thermal resistance; (16) Sample port.

The hot stream of simulated geothermal water stored in a 60 L fluid tank was first heated to a settled temperature and then pumped into the plate heat exchanger by a magnetic force pump. After being cooled by the cold stream of tap water in the heat exchanger, the geothermal water flowed back into the tank. Tap water flowed in the heat exchanger only once. The ion concentrations of simulated geothermal water are listed in Table 1. $CaCO_3$ solution was prepared in an indirect way using calcium chloride ($CaCl_2$) and sodium bicarbonate ($NaHCO_3$).

The materials of the experimental apparatus including the plate heat exchanger are all AISI 304 SS except for gaskets. Chevron corrugated heat transfer plates with or without surface modification of coatings were used. Geometric characteristic parameters of chevron plates are given in Table 2.

Table 1 Ion concentrations of simulated geothermal water.

Ion	Concentration (mg/L)
Na^+	461.6
K^+	71.2
Ca^{2+}	104
Mg^{2+}	38.8
SO_4^{2-}	319.4
HCO_3^-	393.6
Cl^-	420.1
NO_3^-	12.54
Soluble SiO_2	64.5
pH	7.52

Table 2 Parameters of geometric characteristics of chevron plates.

Overall dimension, mm×mm	299×122
Vertical distance between centers of ports, Lv/mm	240
Horizontal distance between centers of ports, Lh/mm	65
Plate width inside gasket, Lw/mm	97
Plate thickness, δ_p/mm	0.7
Port diameter, D_p/mm	25
Corrugation angle, β/°	60
Corrugation pitch, P/mm	9.36
Corrugation amplitude or mean channel width, b/mm	2.4
Projected heat exchanging area, A'/m^2	0.0209
Effective heat exchanging area, A_0/m^2	0.2508
Enlargement factor,ϕ	1.2
Mean flow cross section per channel, fp/m^2	0.000233

The plate heat exchanger consisted of three chevron plates to form one flow channel for geothermal water and one for tap water. In the heat transfer process, hot and cold streams flowed counter-currently. The experimental apparatus were equipped with pressure transducers and platinum resistance thermometers (PT 100) located at the inlets and outlets of the hot and cold fluids. Experimental data including temperature, pressure drop and volume flow rate were recorded every 10 minutes for a 15-day period. The temperatures of hot and cold fluids were measured using four platinum resistance thermometers, and the pressure drop of hot fluid was measured using pressure transducers. The flow rates of hot and cold fluid were measured using rotor flow meter. All of the above elements were connected to a data acquisition system and a computer.

The flow rate of the hot fluid was 140 L/h and its temperature remained 80**℃**. The concentration of simulated geothermal water was kept constant and supersaturated in

$CaCO_3$ solution and filtered with a Y-type filter with the mesh number of 800.

Data treatments

The overall coefficient of convection heat transfer of the plate heat exchanger can be calculated by the method of logarithmic mean temperature difference, as shown in Eq. (1).

$$U = \frac{Q}{A \cdot LMTD} \tag{1}$$

where Q is the heat flux, W； A is the heat exchanger area, m2; LMTD is the logarithmic mean temperature difference for counter-current flow, **°C**, which can be determined

$$LMTD = \frac{(T_2 - T_3) - (T_1 - T_4)}{\ln \frac{(T_2 - T_3)}{(T_1 - T_4)}} \tag{2}$$

where T_1 is the inlet temperature of hot fluid, **°C**; T_2 is the outlet temperature of hot fluid, **°C**; T_3 is the inlet temperature of cold fluid, **°C**; T_4 is the outlet temperature of cold fluid, **°C**.

Heat the hot fluid lost was transferred to the cold fluid and the temperature of the hot fluid decreases. Oppositely, the clod fluid gained heat from the hot fluid and its temperature increases. Heat transfer rate of the hot fluid, Q_h is calculated by Eq.(3) and the rate gained from the hot fluid Qc, is calculated by Eq.(4).

$$Q_h = m_h c_{p,h}(T_1 - T_2) \tag{3}$$

$$Q_c = m_c c_{p,c}(T_4 - T_3) = \rho V_c c_{p,c}(T_4 - T_3) \tag{4}$$

where m_h and m_c (kg/s) represent mass flow rates of hot geothermal water and tap water, respectively. $c_{(p,h)}$ is the specific heat at constant pressure of hot fluid, J/(kg·K); $c_{(p,c)}$ is the specific heat at constant pressure of tap water, J/(kg·K); ρ is the density of the cold fluid, kg/m3; Vc is the volume flow rate of the cold fluid.

If heat loss is zero in convective process, the values of Q_h and Q_c are equal. However, this phenomenon is inevitable in the actual operation process. Hence the thermal equilibrium relative error η is defined to evaluate the thermal equilibrium effects of the heat exchanger. Calculation process is shown in Eq. (5). If η<5-15% (Pantzali, et al., 2009; Xu, 2010), then the experimental data is considered reasonable.

$$\eta = \frac{Q_h - Q_c}{Q_h} \times 100\% \tag{5}$$

In most cases, the heat flux can be calculated by Eq. (6).

$$Q_m = \frac{Q_h + Q_c}{2} \tag{6}$$

But the hot fluid is simulated geothermal water whose inlet temperature is about 80**°C**. The specific heat at constant pressure and the density of simulated geothermal water are difficult to measure accurately. Hence, the rate of heat transfer of cold fluid is considered as the rate of heat rate in this study.

The values of V_c, T_1, T_2, T_3 and T_4 can be recorded by the data acquisition system during the experiment. The overall fouling thermal resistance (R_f / $m^2 \cdot K \cdot W^{-1}$) can be calculated from the Eq. (7).

$$R_f = \frac{1}{U_f} - \frac{1}{U_0} \tag{7}$$

where U_0 and U_f are the overall convection coefficients of the heat exchanger with clean (unfouled) and dirt transfer surfaces which are calculated from Eqs. (1) to (6).

Coatings preparation and characterization

Several coatings were prepared on the plate AISI 304 SS substrates using the liquid phase deposition (LPD) and sol-gel methods and the fouling properties on these surfaces were evaluated.

LPD TiO_2 coatings. Hexafluorotitanate ammonium ($(NH_4)_2TiF_6$) and boric acid (H_3BO_3) were dissolved in deionized water at given temperature and the solution for deposition of the TiO_2 coatings was prepared. The sample was immersed into the deposition solution. After specific reaction time, the sample was taken out from the solution. After being rinsed with deionized water and dried at room temperature, coated sample was subjected to heat treatment. Thus preparation of LPD TiO_2 coatings was finished.

Table 3 Experimental conditions of sol synthesis.

Sol description	Sol 1#	Sol 2#	Sol 3#
	TiO_2	SiO_2	SiO_2-FPS
Alkoxide precursor	TBOT	TBOS	TBOS+PFS
Solvent	C_2H_5OH	C_2H_5OH	C_2H_5OH
Catalyst	-	HCl	HCl
Additive	DEA	DMF	-
Hydrolysis ratio	3	4	4
Precursor concentration, M	0.97	1.37	1.0
Molar ration of HCl	-	0.011	0.011
Remarks	Reacting for 2h at 25 **°C** Aging time: 6h	Reacting for 6h at 60 **°C** Aging time: 7d	Reacting for 6h at 60 **°C** Aging time: 7d

Table 4. The preparation conditions of sol-gel coatings.

Coating sample	Coating preparation
Sol-gel TiO_2 (SS1)	Coated with Sol 1#, sinter at 500**°C** for 2h
Sol-gel TiO_2-FPS (SS2)	(a)Coated with Sol 1#, sinter at 500**°C** for 2h (b)Coated with Sol 3#, sinter at 200**°C** for 2h
Sol-gel SiO_2(SS3)	Coated with Sol 2#, sinter at 500**°C** for 2h
Sol-gel SiO_2-FPS(SS4)	(a)Coated with Sol 2#, sinter at 200**°C** for 2h (b)Coated with Sol 3#, sinter at 500**°C** for 2h

LPD TiO_2-FPS coatings. First, dissolved a certain amount of Fluoroalkylsilane (FPS) in iso-propyl alcohol and then added a small amount of dilute acid into the FPS solution with magnetic stirring. After dehydration, hydrophobic solution was prepared. Then LPD TiO_2 coatings was immersed into the hydrophobic solution and

calcined in the muffle furnace with fixed heating rate. Preparation of LPD TiO_2-FPS coatings was finished.

Sol-gel TiO_2 coatings. The synthesis of the sol-gel solution was based on the hydrolysis of alkoxides. Table 3 shows the experimental conditions of sol synthesis. TiO_2, SiO_2 and SiO_2-FPS sols were obtained referred to as Sol 1#、Sol 2#、Sol 3#, respectively. Sol-gel TiO_2 coatings were obtained by dipping at Sol #1.

Sol-gel TiO_2-FPS coatings. Sol-gel TiO_2-FPS coatings were prepared by two steps: (a) coated with TiO_2 on the substrates by dipping at Sol #1; (b) modified with FPS on the TiO_2 coatings by dipping at Sol #3.

Sol-gel SiO_2 coatings. Sol-gel SiO_2 coatings were obtained by dipping at Sol #2.

Sol-gel SiO_2-FPS coatings. Sol-gel SiO_2-FPS coatings were prepared by two steps: (a) coated with SiO_2 on the substrates by dipping at Sol #2; (b) modified with FPS on the SiO_2 coatings by dipping at Sol #3.

The preparation conditions of sol-gel coatings are listed on Table 4.

RESULTS AND DISCUSSION

Characterization of surfaces

Surface roughness. Surface roughness significantly affects the properties of fouling and corrosion. Corrosive substances are easy to attach to the micro-valleys of rough surface and penetrate to the metal inner layer, cause surface corrosion (Lin and Yan, 2010; Keysar et al.,1994). Meanwhile, micro-convex is easy to become the places of crystal nucleus to induce the fouling deposition. Measured results of surface roughness of various surfaces are shown in Fig. 2. Measured parameters include the mean arithmetic average roughness height (Ra), which is the arithmetic mean of the departures of the roughness profile and the mean roughness depth (Rz), which shows the distance between the highest peak and the lowest valley of roughness profile.

Corrugated 304 SS plate is relatively smooth, and the value of Ra is 0.28 μm. All the roughness values increase except the sol-gel SiO_2 plates, which may be caused by that relatively thick sol-gel SiO_2 coating covered the outline of valley on the plates. Relatively small silica particles can also reduce the surface roughness. Roughness of different coatings changes little after FPS hydrophobic treatment because the thickness of FPS hydrophobic coating is very thin.

Surface free energy. Surface free energy of the plates was calculated according to the contact angles measured by OCA20 optical contact angle measuring instrument with the distilled water, diiodomethane and formamide as standard liquids at 25℃ and image acquisition time of 20s (Correia, et al.,1997; Michalski, et al.,1998). Common calculation methods for solid surface free energy are the Owens-Wendt equation (Rellick and Runt, 1986; Michalski, et al.,1998) and Young-Good-Girifalco-Fowkes equation (van Oss, et al.,1988). Using different standard liquids in Owens-Wendt equationn method can only get the surface free energy of the polar component and non-polar component of solid surface free energy (Rellick and Runt, 1986; Michalski, et al.,1998). However, besides the polar component and non-polar components, using the Young-Good-Girifalco-Fowkes equation method can also get the electron donor γ_i^- and electron acceptor γ_i^+ of the polar component (van Oss, et al.,1988). Accordingly, Young's equation was used in the study. Measured contact angles and calculated surface free energy are displayed in Table 5. As can be seen in Table 5, the un-treated SS hosts the highest surface free energy among all the plate samples, and the surface free energies of the samples which coated with FPS are lower an order of magnitude than others. The surface free energies for those three high-energy surfaces are 41.4mN·m^{-1} for LPD TiO_2 surface, 39.44 mN·m^{-1} for sol-gel TiO_2 surface and 44.94 mN·m^{-1} for sol-gel SiO_2 surface, with the electron donor component γ_i^- of 12.9, 2.45 and 9.54 mN·m^{-1}, respectively. Sol-gel TiO_2-FPS surfaces and sol-gel SiO_2-FPS surfaces show values of the surface free energy of around 8.5mN·m^{-1} with neglectable electron acceptor components, whereas the surface free energy of LPD TiO_2-FPS sample (9.00 mN·m^{-1}) shows much higher electron acceptor component γ_i^-. According to the literature (Wu, et al., 1997; Rosmaninho and Melo, 2006), if the electron donor component γ_i^- is higher, the surface free energy is generally higher. This result is consistent with the literature conclusion.

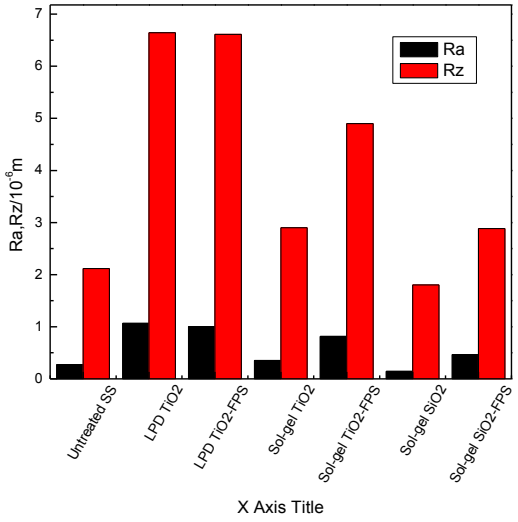

Fig. 2 Surface roughness of different plates.

Table 5 Static contact angle and surface free energy of different plate samples.

Sample	θ_w/°	θ_f/°	θ_d/°	γ_s^{lw}/mN·m^{-1}	γ_s^+/mN·m^{-1}	γ_s^-/mN·m^{-1}	γ_s^{AB}/mN·m^{-1}	γ_s/mN·m^{-1}
un-treated	51.2±2.2	26.2±0.4	33.9±0.5	42.52	1.82	19.39	11.69	54.21
LPD TiO_2	63.7±7.9	42.1±4.3	55.0±4.5	26.80	4.10	12.9	14.60	41.4
LPD TiO_2-FPS	117.1±2.6	111.3±2.2	98.4±7.9	8.20	0.10	2.40	0.80	9.00
Sol-gel TiO_2	79.3±0.9	52.0±1.8	42.6±0.5	37.42	0.48	2.45	2.02	39.44
Sol-gel TiO_2-FPS	120.8±1.4	109.1±0.6	101.8±0.8	8.45	0.06	0.77	0.09	8.54
Sol-gel SiO_2	68.9±2.4	42.8±0.4	44.2±2.0	39.08	2.46	9.54	5.86	44.94
Sol-gel SiO_2-FPS	122.7±0.5	109.1±2.1	100.1±1.6	8.03	0.06	0.22	0.20	8.23

Fouling experiments

Fouling experiments on different coatings were studied. Experiments were conducted at the same thermal fluid temperature and tap water temperature of 9.0-26.0℃ due to change of the room temperature. For comparison, two sets of LPD TiO_2-FPS plates at different pressures were tested. In order to study the reliability of the experiment, LPD TiO_2-FPS plates were operated twice. In each experiment, two of three plates coated with the same coatings formed a thermal fluid channel, and an un-treated plate and one heat exchanger plate formed another channel used as cold fluid channel. The test sections were insulated to minimize heat losses. Table 6 lists the detailed experimental conditions. $T_{h.in}$ and $T_{c.in}$ represent the inlet average temperatures of thermal water and tap water in first four hours, respectively. The initial pressure drop of thermal fluid side in first four hours is represented as *P*.

Table 6 Fouling experimental conditions.

Run No.	Surface	$T_{t.in}$/℃	$T_{c.in}$/℃	P/KPa	Volume flow of fluids/(m^3/h)
1	un-treated	80	9.35	1.90	0.14
2	LPD TiO_2	80	23.25	4.72	0.14
3	LPD TiO_2-FPS	80	27.51	3.38	0.14
4	LPD TiO_2-FPS	80	9.40	1.04	0.14
5	Sol-gel TiO_2	80	28.88	4.57	0.14
6	Sol-gel TiO_2-FPS	80	25.07	6.45	0.14
7	Sol-gel SiO_2	80	27.51	5.93	0.14
8	Sol-gel SiO_2-FPS	80	12.49	0.28	0.14

Fouling on LPD TiO_2 and TiO_2-FPS coatings. The variation trends of fouling resistance with running time on the LPD TiO_2 and TiO_2-FPS coatings are given in Fig. 3.

There is an obvious effect of LPD TiO_2-FPS coatings on antifouling. The plates show the highest reduction in fouling resistance reaching an asymptotic fouling resistance of 1.2×10^{-5} m^2·K/W as compared to 3.3×10^{-5} m^2·K/W for the untreated SS plates after an experimental duration of 17000 min. Furthermore, the fouling induction period of LPD TiO_2-FPS coating plates compared to the untreated SS plates extended three times to 15000min.

As can we see, the slope of the untreated SS fouling curve decrease significantly during the last 100min. The fouling resistance reached a value of 1.7×10^{-5} m^2·K/W，only about half of the value at 17000min. It may assumed that parts of the fouling detached from the metal surface for rinsing by the hot water and that the resulting macro-roughness increased the overall heat transfer coefficient remarkably.

The clean overall heat transfer coefficient of the untreated SS at first 4 hours is 3414 W/(m^2·K). The value of Run 3 is 2565 W/(m^2·K). Two reasons may cause this phenomenon: (1) The thermal conductivity of titania and hydrophobic organics coated on substrate surface are much smaller than the values of the SSl. (2) The initial pressure drop of Run1 (1.90 bar) was lower than the value of Run 3

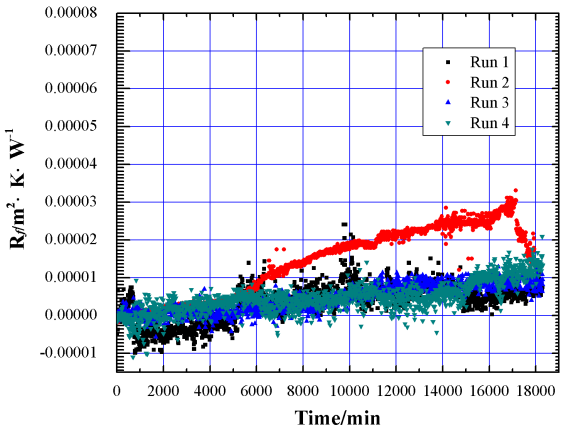

Fig. 3 Effect of LPD TiO_2 and LPD TiO_2-FPS coatings on fouling thermal resistance.

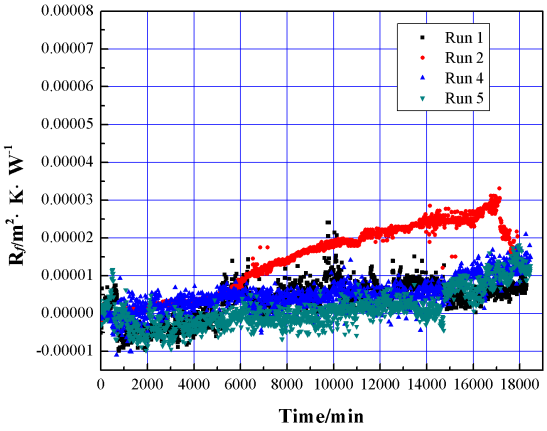

Fig. 4 Effect of LPD TiO_2-FPS coatings on fouling thermal resistance.

(1.04 bar). As we all know when the flow is constant, the larger pressure drop means the faster flow velocity. So resulting in a larger heat transfer coefficient. To investigate, a further experiment was performed using LPD TiO_2-FPS coating plates and increase the initial pressure drop to 3.38 bar (see Fig. 4). The clean overall heat transfer coefficient of the Run4 at first 4 hours increased to 3430 W/(m^2·K). It would therefore appear that the effect of Micro and nano-scale coating on heat transfer can be neglected and the higher flow rate results the higher heat transfer coefficient. Furthermore, two tests of the LPD TiO_2-FPS coating plates show similar asymptotic dirt curve (as shown in Fig. 4). The good repeatability shows the data reliability of the experiment.

Experiment results of Sol-gel coatings. Fig.5 compares the fouling behavior of experiments with two Sol-gel TiO_2 coating surfaces and with an untreated SS surface. At the first 5000min, the fouling resistance for both sol-gel TiO_2 and untreated SS surface is almost zero. This period of time can be considered as fouling induction period. The period of sol-gel TiO_2 plates compare to the untreated SS

plates have no obvious extension. This is followed by an increase period on fouling resistance curve up to the experimental duration of approximately 16000min. After that, the fouling resistance curve rapid increase to 4×10^{-5} $m^2\cdot m$. After that, the fouling resistanc（4×10^{-5} $m^2\cdot m$. A）is a slightly higher than the value of the SS after an experimental duration of 16000min.

This was not expected, as based on the surface energy of the Sol-gel TiO_2 plates, the mount of the deposited salt crystals should be less than in the case of the untreated SS. It would have been expected that the Sol-gel TiO_2 plates show a fouling behavior better than or at least similar to that of the LPD TiO_2 heat exchanger plates due to the measured values of the surface energy and the Lewis acid-base electron donor（γ_s^-）. As can be seen from the images of the Sol-gel TiO_2 plates with corrosion phenomena after the experimental duration of approximately 19000min. On one hand, the thermal conductivity of the corrosion product is usually relatively low. On the other hand, the surface roughness increased after the corrosion. The rougher surface is conducive to fouling deposition. This explains why the experiment results and expectations are not consistent. Analysis the parameters of Run 2 and Run 5 plates, no significant differences in the values of the pressure drop and the surface energy. However, the Sol-gel TiO_2 plates show the lower initial heat transfer coefficient of 2984 $W/(m^2\cdot K)$ as compared to 3218$W/(m^2\cdot K)$ for the LPD TiO_2 plates. It may be assumed that the thickness of the Sol-gel TiO_2 film coated on the plates is thicker than the LPD TiO_2 film.

The fouling behavior of the Sol-gel TiO_2-FPS plates is given in Fig. 5. As can be seen from the fouling resistance curve, the fouling induction period only lasted 3000min, after that no asymptotic trend of the fouling resistance could be observed at all. However, this experiment may help to explain the opposing effects of low surface energy and high surface roughness on the fouling behavior. The surface energy of the Sol-gel TiO_2-FPS plates is approximate to the LPD TiO_2 plates. Therefore, it is most likely the high roughness can provide more number of nucleation sites for the fouling deposition; the high surface roughness has overcome the effect of low surface energy.

Fig. 6 shows the fouling resistance of the sol-gel SiO_2 and the sol-gel SiO_2-FPS plates compare to the curve of the untreated SS verse time diagram during the test period. During the first 6000min of the experimental run, the fouling resistance curves of the two different plates are almost no growth and the fouling resistance values are approximately zero. Fouling induction period increased by 20% relative to the untreated surface. This is beneficial to antifouling. After the 6000min of experimentation, the curves overall trend of plates to be studied increase rapidly, reaching a maximum fouling resistance of 5.8×10^{-5} $m^2\cdot K/W$ and 7×10^{-5} $m^2\cdot K/W$, respectively. During the rise period, the fouling resistance decline intermittently.

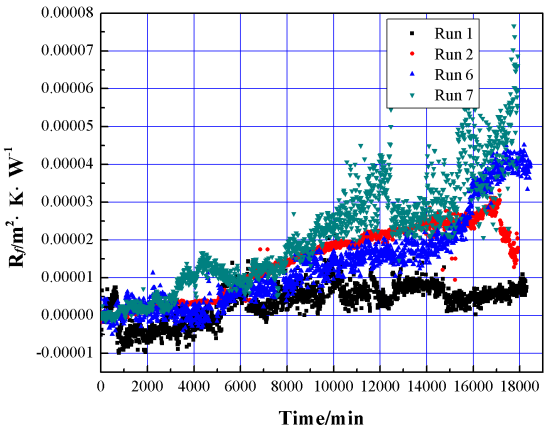

Fig. 5 Effect of sol-gel TiO_2 and sol-gel TiO_2-FPS coatings on fouling thermal resistance.

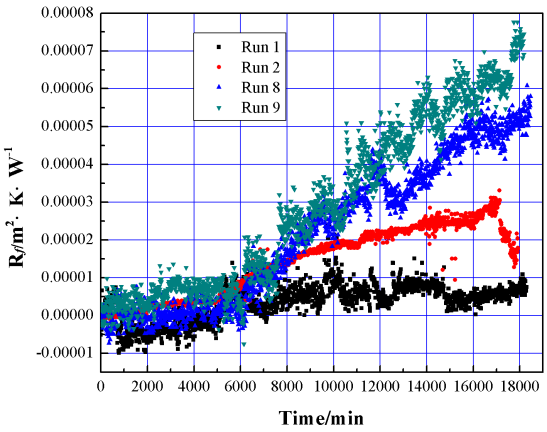

Fig. 6 Effect of sol-gel SiO_2 and sol-gel SiO_2-FPS coatings on fouling thermal resistance.

The investigations by Brant and Childress (2002) and Helalizadeh et al. (2006) have shown that fouling deposition on the heat exchanger surface can be considered as the result of the interaction between the fouling and the heat exchanger surface. Initial fouling deposition rate is strongly dependent on the properties of surface. The surface properties influence fouling deposition when fouling doesn't completely cover the heating surface. Once completely covered, the impact can be ignored. However, if removing fouling from the surface, the surface properties still effect on the process. Final fouling resistance of the Sol-gel SiO_2-FPS coatings plates was about 20% higher than that of the Sol-gel SiO_2 coating plates. This is a good piece of evidence for the point mentioned above. It can be clearly seen from the curves after 6000min, the fouling resistance decline intermittently during the rise period. This phenomenon doesn't occur on the untreated surface. Considering that it may be caused by the following reasons: Fouling deposition is a dynamic process concludes fouling deposition process and fouling stripping process. When the

ISBN: 978-0-9984188-0-3; Published online www.heatexchanger-fouling.com

former rate is higher than the latter rate, the mass of the net deposited fouling increase leads to fouling resistance increase. It also imply that fouling on the studied surface were more loose than that on the untreated one. From the fouling resistance analysis, it may suggest that two different Sol-gel SiO_2 plates is not suitable for antifouling in geothermal water. But, loose and porous deposit breaks easier than the compact deposit and may be washed away by water scouring for a long time. Generally, combined with mechanical cleaning, the Sol-gel SiO_2 and SiO_2-PFS surface will show excellent performance of anti-corrosion and anti-fouling in geothermal water.

CONCLUDINGS

Itemize specific conclusions of the study as follows.

1. There is an obvious effect of LPD TiO_2-FPS coatings with low surface energy on antifouling. The experiments provide evidence for the point of that surface with lower Lewis acid-base electron donor (γ_s^-) would lead to reduced fouling attachment, fewer number of nucleation sites, looser fouling layer easier to remove.
2. Coating with multi-stage structure is not only conducive to formation dense coating with low surface energy to prevent the penetration of corrosive ions but also can improve the binding force of the coating with the substrate.
3. From the fouling resistance analyses, it indicates that two different sol-gel SiO_2 coating plates are not suitable for antifouling in geothermal water. Combined with mechanical cleaning, the sol-gel SiO_2 and SiO_2-PFS coating surfaces will show good performance of anti-corrosion and anti-fouling in geothermal water, although there is no extension of fouling induction period and final fouling thermal resistance increased compares to the untreated SS, loose and porous deposit breaks easier than the compact deposit and may be washed away by fluids.
4. The investigations have signification intimation that using surface engineering technology on heat transfer plates can effectively reduce the fouling deposition. Further work will focus on the mechanism researches and further verification.

ACKNOWLEDGMENTS

The authors thank for the financial support of the National High-Tech Research and Development Projects of China ("863" Program, No. 2012AA052804) and Tianjin Research Program of Application Foundation and Advanced Technology (No. 09JCZDJC24100).

Nomenclature

A_0	effective heat exchanging area, m^2
A'	projected heat exchanging area, m^2
A	heat exchanger area, m^2
b	corrugation amplitude or mean channel width, mm
c	specific heat at constant pressure of fluid, J/(kg·K)
D_p	port diameter, mm
f_p	mean flow cross section per channel, m^2
L_h	horizontal distance between centers of ports, mm
LMTD	logarithmic mean temperature difference for counter-current flow, **℃**
Lv	vertical distance between centers of ports, mm
Lw	plate width inside gasket, mm
m	mass flow rates of fluid, kg/s
P	corrugation pitch, mm
Q	heat flux, W
Ra	mean arithmetic average roughness height, μm
R_f	overall fouling thermal resistance,m^2·K/W
Rz	mean roughness depth, μm
T_1	inlet temperature of hot fluid, **℃**
T_2	outlet temperature of hot fluid, **℃**
T_3	inlet temperature of cold fluid, **℃**
T_4	outlet temperature of cold fluid, **℃**
U_0	overall convection coefficients of the heat exchanger with clean (unfouled) transfer surface
U_f	overall convection coefficients of the heat exchanger with dirt transfer surface
V	volume flow rate of the fluid, m^3/s

Greek Letters

β	corrugation angle, °
δ_p	plate thickness, mm
ϕ	enlargement factor, dimensionless
γ	surface free energy, J/m^2
η	thermal equilibrium relative error, dimensionless
θ	contact angle of solid surface, °
ρ	density of the fluid, kg/m^3

Subscripts and superscripts

h	Hot fluid
c	Cool fluid
+	electron-acceptor component
-	electron-donor component
AB	Lewis acid-base component
LW	nonpolar component

REFERENCES

Amr A G, Schoenbach K H, Biofouling Prevention with Pulsed Electric Fields. Plasma Science, IEEE Transactions on, 2000, 28(1): 115-121.

Axelsson G, Jonasson T, ólafsson M, et al. Successful Utilization of Low-Temperature Geothermal Resources in Iceland for District Heating for 80 Years. Proceedings World Geothermal Congress, Bali, 2010.

Brant JA, Childress AE. Assessing short-range membrane-colloid interactions using surface energetics. Journal of Membrane Science, 2002, 203(1-2): 257-273.

Cai Y W, Liu M Y. Corrosion Behavior of Titania Films Coated by Liquid-Phase Deposition On AISI304 Stainless Steel Substrates. American Institute of Chemical Engineers, 2012, 58(6): 1907-1920.

Cho Y I, Choi B G, Drazner B J. Electronic Anti-Fouling Technology to Mitigate Precipitation Fouling in Plate-and-Frame Heat Exchangers. International Journal of Heat and Mass Transfer, 1998, 41(17): 2565-2571.

Correia NT, Rsmos JJM, Saramago BJV, et al. Estimation of the surface tension of a solid: application to a liquid crystalline polymer. Journal of Colloid and Interface Science, 1997, 189(2): 361-369.

Eliasson E T, Björnsson O B. Multiple Integrated Applications for Low-to Medium-Temperature Geothermal Resources in Iceland. Geothermics, 2003, 32(4): 439-450.

Förster M, Augustin W, Bohnet M. Influence of the Adhesion Force Crystal/Heat Exchanger Surface On Fouling Mitigation. Chemical Engineering and Processing: Process Intensification, 1999, 38(4): 449-461.

Fridleifsson I B. Geothermal Energy for the Benefit of the People. Renewable and Sustainable Energy Reviews, 2001, 5(3): 299-312.

Gallup D L. Investigations of Organic Inhibitors for Silica Scale Control in Geothermal Brines. Geothermics, 2002, 31(4): 415-430.

Gallup D L, Barcelon E. Investigations of Organic Inhibitors for Silica Scale Control From Geothermal Brines-II. Geothermics, 2005, 34(6): 756-771.

Helalizadeh A, Müller Steinhagen H, Jamialahmadi M. Application of fractal theory for characterisation of crystalline deposits. Chemical Engineering Science, 2006, 61(6): 2069-2078.

Hepbasli A, A Key Review On Energetic Analysis and Assessment of Renewable Energy Resources for a Sustainable Future. Renewable and Sustainable Energy Reviews, 2008, 12(3): 593-661.

Hepbasli A, Ozgener L. Development of Geothermal Energy Utilization in Turkey: A Review. Renewable and Sustainable Energy Reviews, 2004, 8(5): 433-460.

Kaya E, Zarrouk S J, O'Sullivan M J. Reinjection in Geothermal Fields: A Review of Worldwide Experience. Renewable and Sustainable Energy Reviews, 2011, 15(1): 47-68.

Keysar S, Semiat R, Hasson D, et al. Effect of Surface Roughness On the Morphology of Calcite Crystallizing On Mild Steel. Journal of Colloid and Interface Science, 1994, 162(2): 311-319.

Kukulka D J, Leising P. Evaluation of Heat Exchanger Surface Coatings. Applied Thermal Engineering, 2010, 30(16): 2333-2338.

Lin C Q，Yan Y Z. Machinery Manufacturing. Beijing: China Machine Press, 2010.

Michalski MC, Hardy J, Saramago BJV. On the surface free energy of PVC/EVA polymer blends: comparison of different calculation methods. Journal of Colloid and Interface Science, 1998, 208(1): 319-328.

Milanovic P, Jacimovic B, Genic S. Experimental Measurement of Fouling Resistance in the Heat Exchanger of a Geothermal Heating System. Geothermics, 2006, 35(1): 79-86.

Pantzali M N, Mouza A A, Paras S V. Investigating the Efficacy of Nanofluids as Coolants in Plate Heat Exchangers (PHE). Chemical Engineering Science, 2009, 64(14): 3290-3300.

Pátzay G, Kármán F H, Póta G. Preliminary Investigations of Scaling and Corrosion in High Enthalpy Geothermal Wells in Hungary. Geothermics, 2003, 32(4): 627-638.

Regenspurg S, Wiersberg T, Brandt W,et al. Geochemical Properties of Saline Geothermal Fluids From the in-Situ Geothermal Laboratory Groß Schönebeck (Germany).Chem Erde-Geochem, 2010, 70: 3-12.

Rellick GS, Runt J. A dielectric study of poly (ethylene-co-vinylacetate)-poly (vinyl chloride) blends. I. Miscibility and phase behavior. Journal of Polymer Science Part B: Polymer Physics, 1986, 24(2): 279-302.

Rosmaninho R, Melo LF. Calcium phosphate deposition from simulated milk ultrafiltrate on different stainless steel-based surfaces. International Dairy Journal, 2006,16(1): 81-87.

Rosmaninho R, Visser H, Melo L. Influence of the Surface Tension Components of Stainless Steel On Fouling Caused by Calcium Phosphate. Trends in Colloid and Interface Science XVI, 2004, 123: 203-209.

Schmitt G. Global Needs for Knowledge Dissemination, Research, and Development in Materials Deterioration and Corrosion Control. World Corrosion Organization, New York, 2009.

Siega F L, Herras E B, Buning B C. Calcite Scale Inhibition: The Case of Mahanagdong Wells in Leyte Geothermal Production Field, Philippines, Antalya, Turkey, 2005.

van Oss CJ, Chaudhury MK, Good RJ. Interfacial Lifshitz-van der Waals and polar interactions in macroscopic systems. Chemical Reviews, 1988,88(6): 279-302.

Wu W, Zhuang H, Nancollas GH. Heterogeneous nucleation of calcium phosphates on solid surfaces in aqueous solution. Journal of Biomedical Materials Research Part A, 1997,35(1): 93-99.

Xu Z M，Guo J S，Guo J S, et al. Experimental study on pressure drop and heat transfer characteristics of plate heat exchanger， Journal of Thermal Science and Technology，2010，9(1).

Zettler H U, Wei M, Zhao Q, et al. Influence of surface properties and characteristics on fouling in plate heat exchanger. Heat Transfer Engineering, 2005, 26(2): 3-17.

Zhang J Y. Control of Trouble in Geothermal Water System Operation. Gas & Heat，1992，6：53-55.

Zhao Q, Liu Y, Müller Steinhagen H, et al. Graded Ni–P–PTFE coatings and their potential applications. Surface and Coatings Technology, 2002,155(2002): 279-284.

Zheng K, Han Z, Zhang Z. Steady Industrialized Development of Geothermal Energy in China-Country Update Report 2005-2009, 2010: 1-11.